THE JOURNAL OF NAVIGATION (2018), **71**, 1247–1262.
doi:10.1017/S0373463318000073

Astronomical Vessel Heading Determination based on Simultaneously Imaging the Moon and the Horizon

Jun-yu Pu, Chong-hui Li, Yong Zheng and Yin-hu Zhan

(Zhengzhou Institute of Surveying and Mapping, Zhengzhou, China, 450001)
(E-mail: lichonghui6501@126.com)

Heading angle is a vital parameter in maintaining a vessel's track along a planned course and should be guaranteed in a stable and reliable way. An innovative method of heading determination based on a fisheye camera, which is almost totally unaffected by electromagnetism and geomagnetism, is proposed in this paper. In addition, unlike traditional astronomical methods, it also has a certain degree of adaptability to cloudy weather. Utilising the super wide Field Of View (FOV) of the camera, it is able to simultaneously image the Moon and the horizon. The Moon is treated as the observed celestial body and the horizon works as the horizontal datum. Two experiments were conducted at sea, successfully proving the feasibility of this method. The proposed heading determination system has the merits of automation, resistance to interference and could be miniaturised, making application viable.

KEYWORDS

1.Vessel. 2. Heading. 3. Fisheye camera. 4. Moon. 5. Horizon.

Submitted: 9 October 2017. Accepted: 3 February 2018. First published online: 30 April 2018.

1. INTRODUCTION. Accurate heading information is critical to the safe navigation of vessels, and to date has usually been achieved by magnetic and gyro compasses. The magnetic compass is sensitive to electromagnetic and geomagnetic variation and deviations, and requires careful calibration and compensation equipment (May, 1948). The gyro compass is widely used at sea and is to some extent not dependent on external circumstances. However, this particular method suffers from its own defect, that of error accumulation. Also, gyroscopes used in vessels are often expensive due to their high quality (Broelmann, 1998). With the rapid development of Global Navigation Satellite Systems (GNSS), GNSS-based heading determination techniques have been developed and this method is relatively simple and reliable (Jurgens, 1990; Graas and Braasch, 1991). However, GNSS-based heading and attitude devices are vulnerable to interference, both to the signals and in extremis to the satellites themselves, and this can be considered as a fatal drawback in extreme cases (Kaplan, 1999; John, 2011).

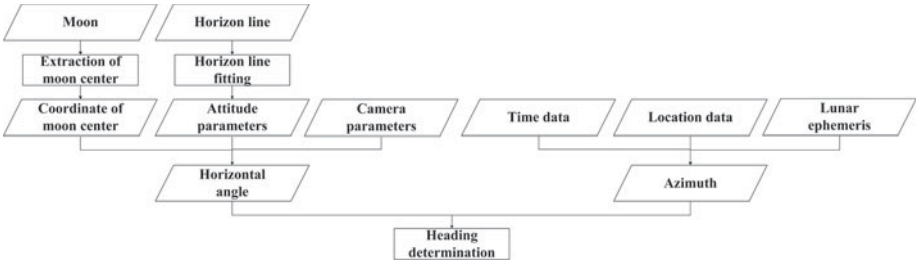

Figure 1. Flowchart of the whole heading determination process.

Passive and stealthy, celestial orientation is a method to determine the azimuth of a vessel or other vehicle through observations of celestial bodies (Hirt et al., 2010; Zhan et al., 2015). Generally, stars are chosen as the observation targets. Unfortunately, on the deck of a vessel, the visibility of stars might be blocked because of clouds in the sky, mist from the sea and light or haze from the vessel itself. The Moon, whose visual magnitude can reach about −12·5 in the full phase (26,000 times brighter than Sirius), is selected here as a substitute for stars. Another problem is the requirement for a horizontal datum, which could be hindered by vessel motion. Inertial units, or other external devices, have been utilised, exacerbating the complexity and expense of the facilities (Levine et al., 1990; US Naval Observatory, 2001). The fisheye camera, whose Field Of View (FOV) can reach or even exceed $180^\circ \times 360^\circ$, was innovatively introduced to simultaneously image the stars and the horizon, determining the Astronomical Vessel Position (AVP) (Li et al., 2012a; 2012b; 2014). In this paper, in order to determine heading, the Moon is chosen as a substitute for stars, and a horizon-fitting algorithm to solve the camera's attitude is proposed. In addition, the fisheye-based heading determination method makes it possible to cover the motion range of the Moon without extra servo control installations, and this characteristic is important for system miniaturisation. Figure 1 shows the whole process of Moon-observing heading determination from a macro perspective, which will be elaborated in the following sections.

2. TRANSFORMATION FROM IMAGE SPACE TO OBJECT SPACE. Figure 2 shows the transformation mechanism between image space and object space when taking observations using the fisheye camera. In Figure 2, P is the point in image space, P' is the point in object space, O' is the intersection between the principal optic axis and image plane, named the principal point. $O\text{-}X_cY_cZ_c$ is defined as the camera coordinate system, in which the origin O represents the optical centre of the camera, axis Z_c coincides with the principal optic axis, axis X_c is perpendicular to axis Z_c and parallel to axis x of the image plane coordinate system and finally axis Y_c is determined by the right-hand rule. As is demonstrated, A_c is defined as the intersection angle between the vertical plane through P' and the plane X_cOZ_c is named azimuth, and θ_c is defined as the intersection angle between the vector through P' and the axis Z_c, named the semi-angular field. Theoretically, point P' could be determined with A_c and θ_c.

To achieve precise conversion between coordinates in object space and image space, a projection model and a distortion model of the fisheye lens must be constructed. Normally, fisheye projection models include an equidistance projection model, an equisolid projection

https://doi.org/10.1017/S0373463318000073 Published online by Cambridge University Press

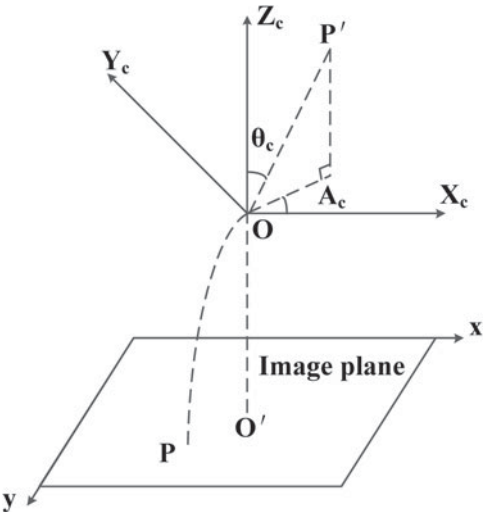

Figure 2. Principle of lens projection.

model, a stereoscopic projection model, and an orthogonal projection model, etc. (Wang, 2006). In this paper, the lens chosen in experiments complies with the equisolid projection model. In addition, unlike in Gaussian optics, the "non-similar" theory is applied to the fisheye lens to meet the requirements of a super-wide FOV. Therefore, a distortion model is needed. Normally, the optical distortion of the fisheye lens could be divided into radial distortion, eccentric distortion and in-plane distortion. Among these, the eccentric and in-plane distortions are in the magnitude of $10^{-5} \sim 10^{-7}$ when compared with radial distortion, and thus they can be neglected. In order to describe radial distortion, a fourth order polynomial is used in this paper, which is shown as follows (Yuan, 2012):

$$\theta_c = 2\arcsin\frac{r}{2f} + k_1\left(\arcsin\frac{r}{2f}\right)^2 + k_2\left(\arcsin\frac{r}{2f}\right)^3 + k_3\left(\arcsin\frac{r}{2f}\right)^4 \quad (1)$$

Where, θ_c denotes the semi-angular field of object point P', f denotes the focal length of the fisheye camera, (k_1, k_2, k_3) denotes the radial distortion parameters, r denotes the distance between image point P and principal point O' in the image plane, which is defined as

$$r = \sqrt{(x - x_0)^2 + (y - y_0)^2} \quad (2)$$

(x, y) denotes image point P's coordinates in the image plane, and (x_0, y_0) denotes principal point O''s coordinates in the image plane.

In the image plane, the intersection angle between vector PO' and axis x is equivalent to the azimuth of P' in the camera coordinate system. Therefore, A_c can be calculated as

$$A_c = \begin{cases} \arctan\dfrac{y - y_0}{x_0 - x} & x_0 - x > 0, y - y_0 > 0 \\ \arctan\dfrac{y - y_0}{x_0 - x} + \pi & x_0 - x < 0 \\ \arctan\dfrac{y - y_0}{x_0 - x} + 2\pi & x_0 - x > 0, y - y_0 < 0 \end{cases} \quad (3)$$

https://doi.org/10.1017/S0373463318000073 Published online by Cambridge University Press

(A_c, θ_c) could be converted to Three-Dimensional (3D) Cartesian coordinates as follows:

$$\mathbf{S}_c = \begin{bmatrix} x_c \\ y_c \\ z_c \end{bmatrix} = \begin{bmatrix} \sin\theta_c \cos A_c \\ \sin\theta_c \sin A_c \\ \cos\theta_c \end{bmatrix} \tag{4}$$

3. EXTRACTION OF THE MOON CENTRE IN THE IMAGE PLANE. The average flattening of the Moon is approximately 1/3,476, and the lunar geometric centre does not coincide with its centroid because the centroid is biased about 2 km towards the earth (Ouyang, 2005; Li et al., 2012b). However, due to the long distance between the Moon and the Earth, the Moon disk observed on the Earth could be approximately considered as circular, with an angular radius of about 15′.

3.1. *Algorithm to fit the Moon centre.* Generally, a circular target will present an approximate ellipse on the image plane when shot by a fisheye camera. Furthermore, with the increase of the semi-angular field, the target's image will get closer to the boundary of the FOV, and the ellipticity will become more obvious. Similarly, the lunar edge line is certain to form an approximate ellipse on the image plane. To fit the centre of the Moon, an algorithm—Direct Least Squares Fitting of Ellipses (DLS), is introduced, whose fundamental idea is briefly conveyed as follows (Fitzgibbon et al., 1996).

The general Equation of an ellipse is

$$F(x,y) = ax^2 + bxy + cy^2 + dx + ey + f = 0, b^2 - 4ac < 0 \tag{5}$$

The inequality constraint $b^2 - 4ac < 0$ could be changed as an equality constraint $4ac - b^2 = 1$.

By introducing vectors

$$\mathbf{A} = (a,b,c,d,e,f)^T \quad \mathbf{P} = (x^2, xy, y^2, x, y, 1) \tag{6}$$

$F(x,y)$ could be rewritten as the vector form

$$F_{\mathbf{A}}(\mathbf{P}) = \mathbf{PA} \tag{7}$$

$|F_{\mathbf{A}}(\mathbf{P}_i)|$ is defined as the algebraic distance of the point (x_i, y_i) to the fitting ellipse $F(x,y) = 0$, which reflects the fitting residual error at the point (x_i, y_i). Then a vector formed by algebraic distances of all the fitting participants can be created, whose norm can be regarded as a fitting accuracy index. The specific vector **A** minimising the norm mentioned above is the direct least squares fitting value of elliptic coefficients.

Suppose the number of points participating in elliptical fitting is M, the coordinates of the points are $(x_1, y_1) \ldots (x_M, y_M)$. By introducing matrices

$$\mathbf{D} = \begin{pmatrix} x_1^2 & x_1y_1 & y_1^2 & x_1 & y_1 & 1 \\ \vdots & \vdots & \vdots & \vdots & \vdots & \vdots \\ x_i^2 & x_iy_i & y_i^2 & x_i & y_i & 1 \\ \vdots & \vdots & \vdots & \vdots & \vdots & \vdots \\ x_M^2 & x_My_M & y_M^2 & x_M & y_M & 1 \end{pmatrix} \quad \mathbf{C} = \begin{pmatrix} 0 & 0 & 2 & 0 & 0 & 0 \\ 0 & -1 & 0 & 0 & 0 & 0 \\ 2 & 0 & 0 & 0 & 0 & 0 \\ 0 & 0 & 0 & 0 & 0 & 0 \\ 0 & 0 & 0 & 0 & 0 & 0 \\ 0 & 0 & 0 & 0 & 0 & 0 \end{pmatrix} \tag{8}$$

https://doi.org/10.1017/S0373463318000073 Published online by Cambridge University Press

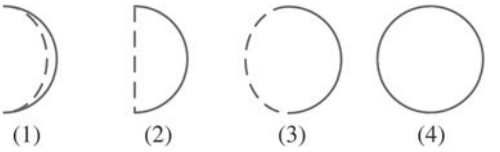

Figure 3. Moon phase.

the fitting assignment can be rewritten as (Halif and Flusser, 1998)

$$\min_{\mathbf{A}} \|\mathbf{DA}\| \quad st \quad \mathbf{A}^{\mathbf{T}}\mathbf{CA} = 1 \tag{9}$$

which can be solved by generalised eigenvectors

$$\begin{cases} \mathbf{D}^{\mathbf{T}}\mathbf{DA} = \lambda\mathbf{CA} \\ \mathbf{A}^{\mathbf{T}}\mathbf{CA} = 1 \end{cases} \tag{10}$$

It can be proved that Equation (10) has a sole positive eigenvalue λ, whose corresponding eigenvector is exactly the coefficient vector of the best-fit ellipse for the given set of points (Gander, 1981).

3.2. *Method to vote in the real edge line of the Moon phase.* The Moon has a periodic phase change when observed from the Earth. The Moon phase is composed of a twilight demarcation line and a real edge line, in which only the real edge line can be used to extract the lunar centre. As a consequence, it is necessary to distinguish the two respective lines.

Normally, such problems tend to be solved by means of robust estimation, for example, the method named Random Sample Consensus (RANSAC), whose basic idea is to search for a best-fit model utilising inliers mixed up with outliers (Fischler and Bolles, 1981; Hast et al., 2013). However, for the Moon, the outliers (the twilight demarcation line) appear to frequently vote for a regular curve, therefore, this method might occasionally become invalid. Furthermore, for better results, the setting of thresholds might have to be artificially changed with the Moon phase cycle, which is considered to be a serious obstacle in engineering practice. In order to overcome these problems and vote in the real edge line accurately and adequately, a two-step scheme is proposed, which includes a half-intercepted search for preliminary voting and a cyclic search for refinement voting. Making use of the feature of the Moon phase, this method demonstrates good effectiveness and stability.

3.2.1. *Half-intercepted Search.* Figure 3 is a sketch of the Moon's phases, in which the solid line denotes the real edge line and the dotted line denotes the twilight demarcation line, whose length is always shorter than that of the former. For that reason, if intercepting a half quantity of total Moon edge points as the search step, taking the norm of the algebraic distance vector ($\|\mathbf{DA}\|$ in Equation (9)) as the ellipse fitting accuracy index, the specific half point set minimising the norm will definitely belong to the lunar real edge line. The implementation steps are carried out as follows:

(1) Suppose the total number of edge points detected from the Moon phase is N, a half-rounded continuous quantity ($[N/2]$) of points are expected to be intercepted for ellipse fitting;

https://doi.org/10.1017/S0373463318000073 Published online by Cambridge University Press

(2) $[N/2]$ is designated as the length of the search step, during which the search should be kept underway until the step coincides with the first one chosen. In this way, ellipse fitting is repeated N times;
(3) Calculate the norms of the algebraic distance vectors;
(4) The set of points corresponding to the minimal norm are the ones preliminarily voted in.

3.2.2. *Cyclic Search.* The majority of points on the real edge line of the Moon phase can be voted in utilising the method above. However, if we fit the Moon centre merely with them, part of the precision may be lost. Considering this, a further search for the points left should be implemented. To achieve this, a cyclic search method is proposed based on the average of algebraic distances. The detailed implementation steps are carried out as follows:

(1) Suppose the total number of Moon phase edge points is N, the real edge points preliminarily voted in are (x_1, y_1), (x_2, y_2), ..., (x_i, y_i), ..., $(x_{[N/2]}, y_{[N/2]})$, and the coefficient vector of the fitting ellipse is A_1. By introducing vector

$$\mathbf{P}_i = (x_i^2, x_i y_i, y_i^2, x_i, y_i, 1) \tag{11}$$

the average of algebraic distances from these points to the fitting ellipse can be expressed as

$$\overline{d}_1 = \frac{1}{[N/2]} \sum_{i=1}^{[N/2]} |\mathbf{P_i A_1}| \tag{12}$$

(2) Suppose one specific point left after the preliminary search process is (x_t, y_t). By introducing vector

$$\mathbf{P}_t = (x_t^2, x_t y_t, y_t^2, x_t, y_t, 1) \tag{13}$$

the algebraic distance from this point to the fitting ellipse in step (1) is

$$d_t = \left| F_{\mathbf{A_1}}(\mathbf{P}_t) \right| = |\mathbf{P_t A_1}| \tag{14}$$

(3) If $d_t < \overline{d}_1$, point (x_t, y_t) can be treated as one of the Moon's real edge points.
(4) Suppose there are W qualified points voted in from step (3). Arriving here, $[N/2] + W$ real edge points can be obtained, including (x_1, y_1), (x_2, y_2), ..., (x_i, y_i), ..., $(x_{[N/2]+W}, y_{[N/2]+W})$. Using these points for the second elliptical fit, the coefficient vector received is A_2. Similarly, the average of algebraic distances from these points to the latest fitting ellipse are expressed as

$$\overline{d}_2 = \frac{1}{[N/2] + W} \sum_{i=1}^{[N/2]+W} |\mathbf{P_i A_2}| \tag{15}$$

(5) Calculate the algebraic distances from the points still left to the latest fitting ellipse and determine whether they belong to the Moon's real edge line, just as step (2) and step (3) have conducted. Steps (2)-(4) should be repeated until no point could be voted in from step (3). Arriving here, the real edge line of the Moon could be considered to be completely discovered.

Figure 4 is a flowchart of the process described above.

https://doi.org/10.1017/S0373463318000073 Published online by Cambridge University Press

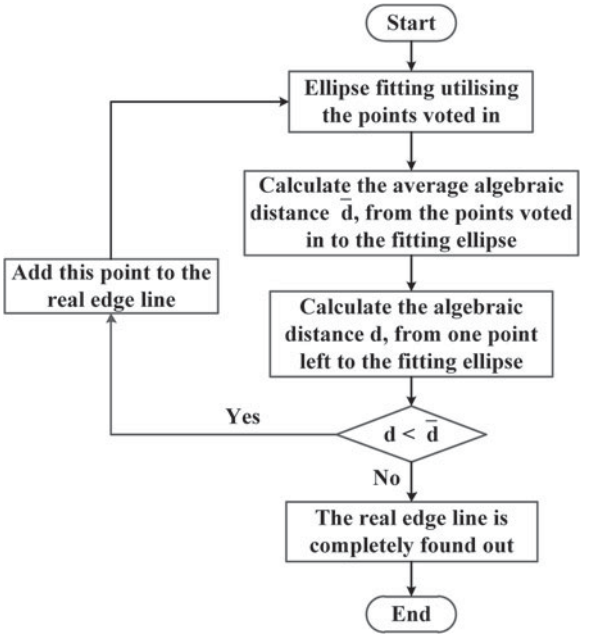

Figure 4. Flowchart of cyclic search.

4. VESSEL ATTITUDE DETERMINATION BASED ON OBSERVATION OF THE HORIZON. According to the method described above, the coordinates of the Moon centre on the image plane can be extracted and can be further converted to camera coordinates. In order to achieve a Moon-observing heading determination, the coordinates of the Moon centre should be revised to the horizontal plane. The horizon is a natural intersection between the sky and the water at sea, which supplies a natural horizontal datum perpendicular to the local plumb line (Li et al., 2016). Given this beneficial condition, an algorithm to solve the camera's attitude based on horizon observation is proposed.

In Figure 5, O is the camera optical centre, OA and OB are two lines of view for the observation of the horizon, which are at a tangent to the sea at points A and B. All the tangent points constitute a horizontal circle, where O' is the centre, r is the radius, and E is the geocentre. OS is perpendicular to the sea surface, and point S is located on the sea surface. The length of OS is h.

In ΔOAE, $\angle OAE$ is a right angle, then

$$|OA| = \sqrt{|OE|^2 - |AE|^2} = \sqrt{(R+h)^2 - R^2} = \sqrt{h^2 + 2Rh} \tag{16}$$

$\angle OO'A$ is right angle, then

$$r = |O'A| = \frac{|OA| \cdot |AE|}{|OE|} = \frac{R\sqrt{h^2 + 2Rh}}{R+h} \tag{17}$$

Figure 6 is a sketch for the camera shooting the horizon, in which O-$X_cY_cZ_c$ is the camera coordinate system. O-$X_{ch}Y_{ch}Z_{ch}$ is defined as the camera horizontal coordinate system. In the camera horizontal coordinate system, origin O is the optical centre of the camera, axis

https://doi.org/10.1017/S0373463318000073 Published online by Cambridge University Press

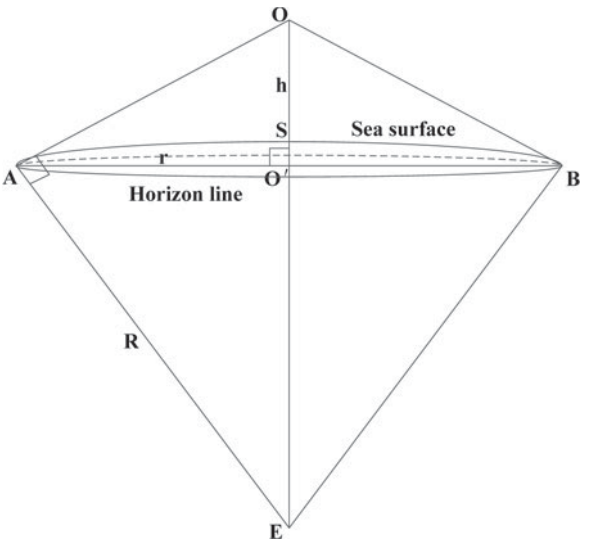

Figure 5. Principle of horizon observation.

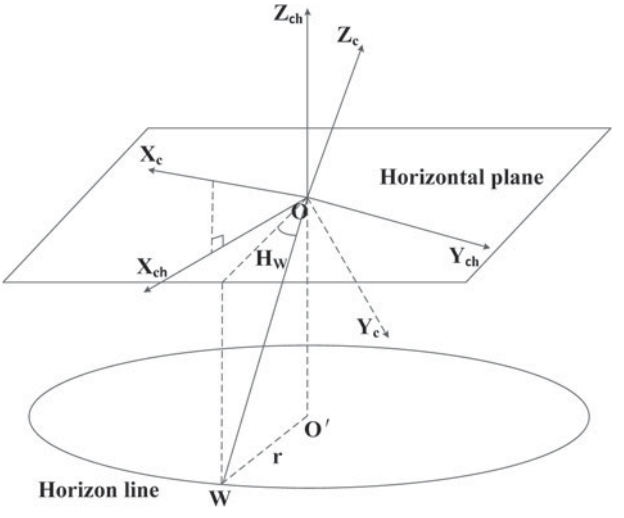

Figure 6. Relationship between coordinate systems.

Z_{ch} points to the zenith, axis X_{ch} is axis X_c's projection on the horizontal plane and axis Y_{ch} is determined by the right-hand rule. W is a point on the horizon and H_W is the elevation angle of W in the camera horizontal coordinate system.

Two steps are required for the transformation from O-$X_cY_cZ_c$ to O-$X_{ch}Y_{ch}Z_{ch}$:

(1) Rotate γ radians around axis X_c, and the rotation matrix can be expressed as $\mathbf{R}_X(\gamma)$;
(2) Rotate ψ radians around axis Y_c, and the rotation matrix can be expressed as $\mathbf{R}_Y(\psi)$;

https://doi.org/10.1017/S0373463318000073 Published online by Cambridge University Press

$\mathbf{R}_c^{ch}$ is defined as the rotation matrix from $O\text{-}X_cY_cZ_c$ to $O\text{-}X_{ch}Y_{ch}Z_{ch}$, which can be calculated as

$$\mathbf{R}_c^{ch} = \mathbf{R}_Y(\psi)\mathbf{R}_X(\gamma) \tag{18}$$

Its holonomic form is

$$\mathbf{R}_c^{ch} = \begin{bmatrix} \cos\psi & \sin\psi\sin\gamma & -\sin\psi\cos\gamma \\ 0 & \cos\gamma & \sin\gamma \\ \sin\psi & -\cos\psi\sin\gamma & \cos\psi\cos\gamma \end{bmatrix} \tag{19}$$

$\mathbf{S}_c$ denotes the 3D vector of point W in the camera coordinate system and it can be transformed into the camera horizontal coordinate system as:

$$\mathbf{S}_{ch} = \begin{bmatrix} x_{ch} \\ y_{ch} \\ z_{ch} \end{bmatrix} = \mathbf{R}_c^{ch} \cdot \mathbf{S}_c = \begin{bmatrix} x_c\cos\psi + y_c\sin\psi\sin\gamma - z_c\sin\psi\cos\gamma \\ y_c\cos\gamma + z_c\sin\gamma \\ x_c\sin\psi - y_c\cos\psi\sin\gamma + z_c\cos\psi\cos\gamma \end{bmatrix} \tag{20}$$

The tangent of point W's elevation angle is

$$\tan H_W = \frac{z_{ch}}{\sqrt{x_{ch}^2 + y_{ch}^2}} \tag{21}$$

In fact, H_W is equivalent to the value of $\angle OAO'$. Furthermore, in Figure 5, it is clear that $\angle OAO' = \angle OEA$. So the following equation can be deduced

$$\tan H_W = \frac{|OA|}{|AE|} = \frac{\sqrt{h^2 + 2Rh}}{R} \tag{22}$$

By combining Equations (21) and (22), the following relationship can be established:

$$\frac{z_{ch}^2}{x_{ch}^2 + y_{ch}^2} = \frac{h^2 + 2Rh}{R^2} \tag{23}$$

Then the error equation for least square estimation can be written as

$$v = \frac{z_{ch}^2}{x_{ch}^2 + y_{ch}^2} - \frac{h^2 + 2Rh}{R^2} \tag{24}$$

which includes only two unknown parameters, namely, the pitch angle ψ and the roll angle γ. The holonomic form of Equation (24) is

$$v = f(\psi, \gamma) = \frac{(x_c\sin\psi - y_c\cos\psi\sin\gamma + z_c\cos\psi\cos\gamma)^2}{(x_c\cos\psi + y_c\sin\psi\sin\gamma - z_c\sin\psi\cos\gamma)^2 + (y_c\cos\gamma + z_c\sin\gamma)^2} - \frac{h^2 + 2Rh}{R^2} \tag{25}$$

Linearizing Equation (25), and taking the initial value $\mathbf{X}_0 = \begin{bmatrix} \psi_0 & \gamma_0 \end{bmatrix}^T$ for the two unknown parameters, the error equation can be represented as

$$\mathbf{V} = \mathbf{A}\delta\hat{\mathbf{X}} + \mathbf{L} \tag{26}$$

In Equation (26), $\mathbf{V}$ is the residual vector, $\mathbf{A}$ is the coefficient matrix, $\delta\hat{\mathbf{X}}$ is the correction vector for unknown parameters, and $\mathbf{L}$ is the free vector for the error equation. A detailed interpretation of Equation (26) is presented in the Appendix.

https://doi.org/10.1017/S0373463318000073 Published online by Cambridge University Press

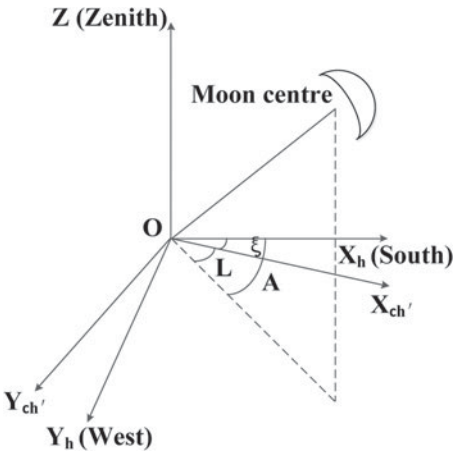

Figure 7. Principle of heading determination by lunar observation.

Based on the least squares criterion, the estimated vector of the attitude parameters can be calculated as

$$\hat{\mathbf{X}} = -(\mathbf{A}^T\mathbf{A})^{-1}\mathbf{A}^T\mathbf{L} + \mathbf{X}_0 \tag{27}$$

The process above requires iterative calculations. Generally, the two attitude parameters do not fluctuate more than $\pm 10^\circ$ and they are sensitive to observations. Therefore, in the normal calculation process, the initial values of the parameters can be taken conveniently as 0, and the residual error can be controlled below $0{\cdot}1''$ by iterating 4∼5 times.

5. METHOD TO RESOLVE THE HEADING ANGLE. The Moon centre position on the image plane can be transformed into the camera coordinate system utilising the projection model and distortion model presented in Section 2. Then utilising the camera attitude parameters calculated by the method presented in Section 4, the Moon centre position will be further transformed into the camera horizontal coordinate system. In order to establish contact with the horizon coordinate system (defined as a left-handed system here), the axis Y_{ch} of the camera horizontal coordinate system should be reversed for conversion to a left-handed system. Figure 7 is a sketch reflecting the key principle of heading determination by lunar observation, where O denotes the camera's optical centre, O-X_hY_hZ denotes the horizon coordinate system, and O-$X_{ch'}Y_{ch'}Z$ denotes the converted camera horizontal coordinate system (left-handed system), which share axis Z with the horizon coordinate system. At the moment of camera exposure, L is the horizontal angle of the Moon centre in O-$X_{ch'}Y_{ch'}Z$, and A is its azimuth in O-X_hY_hZ. ξ is the heading angle—the intersection angle between $X_{ch'}$ and X_h. Also, ξ is equal to the intersection angle between the projection of axis X_c on the horizontal plane and the south direction.

The formula to calculate heading angle is

$$\xi = A - L \tag{28}$$

We now briefly introduce the calculation process for horizontal angle L.

https://doi.org/10.1017/S0373463318000073 Published online by Cambridge University Press

Suppose $\mathbf{S}_{ch'}$ is the vector of the Moon centre in $O\text{-}X_{ch'}Y_{ch'}Z$, which can be calculated as

$$\mathbf{S}_{ch'} = \begin{bmatrix} x_{ch'} \\ y_{ch'} \\ z_{ch'} \end{bmatrix} = \mathbf{P}_Y \mathbf{R}_c^{ch} \mathbf{S}_c \tag{29}$$

In Equation (29), $\mathbf{S}_c$ can be obtained from Equation (4), $\mathbf{R}_c^{ch}$ can be obtained from Equation (19), and $\mathbf{P}_Y$ is the reversal matrix of axis Y. Therefore, L can be calculated as

$$L = \begin{cases} \arctan \dfrac{y_{ch'}}{x_{ch'}} & x_{ch'} > 0, y_{ch'} > 0 \\ \arctan \dfrac{y_{ch'}}{x_{ch'}} + \pi & x_{ch'} < 0 \\ \arctan \dfrac{y_{ch'}}{x_{ch'}} + 2\pi & x_{ch'} > 0, y_{ch'} < 0 \end{cases} \tag{30}$$

As for the azimuth A, it can be calculated taking advantage of the exposure moment, the lunar ephemeris and the vessel's location. Generally, the hour angle method is used to solve this (Adams, 1968; Robbins, 2013).

$$\tan A = \frac{\cos \delta \sin t}{\sin \varphi \cos \delta \cos t - \sin \delta \cos \varphi} \tag{31}$$

In Equation (31), φ is the astronomical latitude of the vessel, δ is the lunar declination, and t is the lunar hour angle, which can be calculated as

$$t = S_0 + T_{\text{ut1}} + \lambda - \alpha \tag{32}$$

In Equation (32), α is the lunar right ascension and λ is the astronomical longitude of the vessel. The AVP written as (φ, λ) can be obtained from sequential shooting of the Moon and information from the inertial navigation system about relative movement during the shooting. T_{ut1} is the Greenwich Universal Time (UT1) at the camera exposure moment, which should be calculated from Coordinated Universal Time (UTC) and the Earth orientation parameter —UT1-UTC. The former is recorded by a high-precision timer and the latter is received from the bulletin communique issued regularly by International Earth Rotation Service (IERS). S_0 is the Greenwich sidereal time when the UT1 becomes zero.

6. EXPERIMENT ANALYSIS. To test the reliability of the heading determination method, two experiments were carried out. The first was conducted in Huanghai coastal waters on the night of 31 October 2012, while the second was in Bohai Bay on the night of 13 July 2017.

The Charge Coupled Devices (CCD) used in the two experiments were different, notably in the array size (3056 × 3056 pixel and 2048 × 2048 pixel respectively) and the quantum efficiency (64% and 96% respectively). The weather conditions during the two experiments met the demand - good visibility of both the Moon and the stars. However, there was a little mist on the sea surface. Fortunately, under moonlight illumination, the observation of the horizon was almost unaffected. Since the ship was always in a state of roll, the heading angle varied from time to time. Thus, it was difficult to obtain the true value of heading angle at the camera exposure moment. To solve this, the average heading result

https://doi.org/10.1017/S0373463318000073 Published online by Cambridge University Press

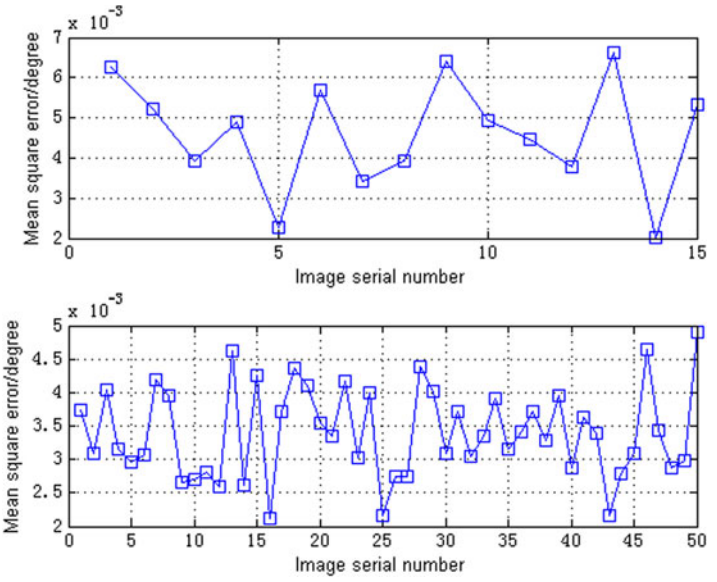

Figure 8. Results of star-observing heading determination.

from hundreds of stars was taken as a reference to evaluate the accuracy of Moon-observing heading determination.

During the 31 October 2012 experiment, 15 images were collected, while the number was 50 for the 13 July 2017 experiment. Figure 8 demonstrates the mean square error of heading angle for each image calculated from multiple stars, and the fluctuation ranges are $2{\cdot}0 \times 10^{-3} \sim 6{\cdot}6 \times 10^{-3}\,^{\circ}$ and $2{\cdot}1 \times 10^{-3} \sim 4{\cdot}9 \times 10^{-3}\,^{\circ}$ respectively. Among the former 15 images, the average mean square error is $4{\cdot}6 \times 10^{-3}\,^{\circ}$, while the magnitude of error in the later 50 images is $3{\cdot}4 \times 10^{-3}\,^{\circ}$. Both experiments fully meet the accuracy demand for a vessel's heading and can act as a reference for Moon-observing heading determination. The accuracy of the 13 July 2017 experiment seems to be a little higher, which could be attributed to the CCD's better photosensitive performance, that is, the higher quantum efficiency may help the camera alleviate the influence of fog and clouds, and thus it can capture a clearer horizon and more stars, contributing to more stable and reliable results.

The data in Figure 9 show the deviation of heading results between the Moon and the stars for each image. As is indicated in the upper figure, the deviations of the 31 October 2012 experiment vary from $-0{\cdot}045^{\circ}$ to $0{\cdot}026^{\circ}$. Similarly, the situation for the 13 July 2017 experiment in the lower figure is $-0{\cdot}047^{\circ}$ to $0{\cdot}04^{\circ}$. In addition, the average deviations of the two experiments are $0{\cdot}021^{\circ}$ and $0{\cdot}019^{\circ}$, respectively. As can be seen from the two graphs, in general, the results of Moon-observing heading determination have stable randomness, mainly fluctuating in the range of $-0{\cdot}04^{\circ} \sim 0{\cdot}04^{\circ}$ and $-0{\cdot}05^{\circ} \sim 0{\cdot}05^{\circ}$. Following this, the results of the first experiment tended to behave more steadily, and this is probably because the higher resolution ratio of the CCD (3056×3056 pixel) can give a larger Moon image in the image plane, which is helpful for the extraction of the Moon's centre.

In general, the heading errors can be generated by methodological, algorithmic, environmental or hardware causes. Normally, the main possible error causes are:

https://doi.org/10.1017/S0373463318000073 Published online by Cambridge University Press

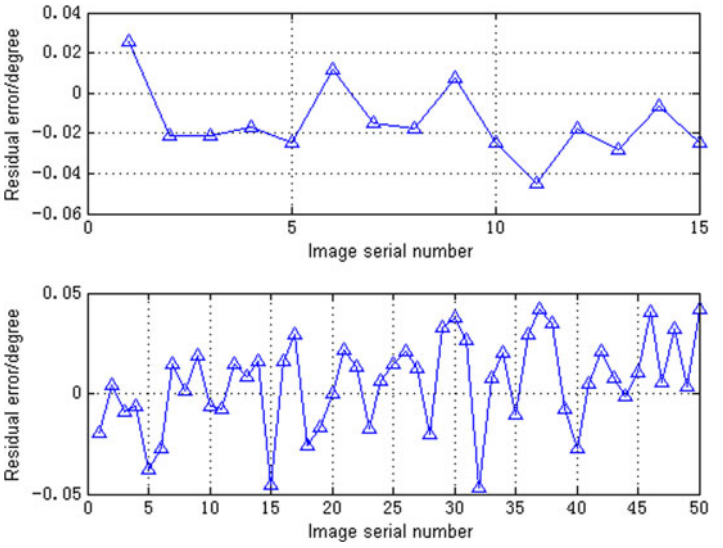

Figure 9. Results of Moon-observing heading determination.

(1) The elevation angle of the Moon changes over time, and the magnitude of influence on the horizontal angle L from the tangential component of the lunar centre extraction error may change with elevation angle.
(2) The horizon extraction error may lead to a systematic deviation of camera attitude parameters, further contributing to the L error.
(3) The inaccurate camera parameters (especially the principal point's coordinate (x_0, y_0)), stemming from the camera calibration error or parameter drift caused by changes in environmental factors (temperature, humidity, air pressure, etc.), may lead to the L error.

7. CONCLUSION. This paper focuses on a heading determination method using simultaneous imaging of the Moon and the horizon. A fisheye camera is utilised to achieve a super-wide FOV. A two-step scheme is proposed to vote in the real edge line of the Moon's phase, and a Direct Least Squares Fitting of Ellipses algorithm is introduced to fit the Moon's centre. Furthermore, a fitting algorithm for the horizon to solve the camera's attitude is proposed. Finally, the fundamental principle to resolve the heading angle is presented. Results from two different experiments indicate that the average deviation between our Moon-observing method and star-observing methods is approximately 0.02°. The main characteristics of this method are:

(1) Automatic operation. All the procedures can be completed by a fisheye camera and a portable computer without manual intervention. The camera is responsible for shooting and the computer undertakes control and processing.
(2) High-level anti-interference. This method has largely removed the restrictions of electromagnetism and geomagnetism. Furthermore, it could also weaken the influence of cloudy weather, to some extent.

https://doi.org/10.1017/S0373463318000073 Published online by Cambridge University Press

(3) Miniaturised system. The super-wide FOV of the fisheye camera can ensure coverage of the Moon and the horizon, avoiding the introduction of an external servo or horizon devices.

Finally, it should be pointed out that the Moon is just regarded as a stable example for observation; the stars could also be used as available observing targets in permissible conditions, which can help greatly improving heading precision, especially when the Moon is not visible.

FINANCIAL SUPPORT

This work was supported by Natural Science Foundation of China under grants NO.11673076, NO. 41604011 and; NO. 41704006.

REFERENCES

Adams, L. P. (1968). Astronomical Position and Azimuth by Horizontal Directions. *Survey Review*, **19**(148), 242–251.

Broelmann, J. (1998). The Development of the Gyrocompass – Inventors as Navigators. *Journal of Navigation*, **51**(2), 267–273.

Fischler, M. A. and Bolles, R. C. (1981). Random Sample Consensus: A Paradigm for Model Fitting with Applications to Image Analysis and Automated Cartography. *Communications of the ACM(Association for Computing Machinery)*, **24**(6), 381–395.

Fitzgibbon, A. W., Pilu, M. and Fischer, R. B. (1996). Direct Least Squares Fitting of Ellipses. *Proceedings of the 13th International Conference on Pattern Recognition*, Vienna, CA.

Gander, W. (1981). Least Squares with a Quadratic Constraint. *Numerische Mathematik*, **36**(3), 291–307.

Graas, F.V., and Braasch, M. (1991). GPS Interferometric Attitude and Heading Determination: Initial Flight Test Results. *Navigation*, 38(4), 297–316.

Halif, R., and Flusser, J. (1998). Numerically Stable Direct Least Squares Fitting of Ellipses. *Proceedings of the. 6th International Conference in Central Europe on Computer Graphics and Visualization*, Plzeň, CA.

Hirt, C., Burki, B., Somieski, A., and Seeber, G. (2010). Modern Determination of Vertical Deflections Using Digital Zenith Cameras. *Journal of Surveying Engineering*, **136**(1), 1–12.

Hast, A., Nysjö, J., and Marchetti, A. (2013). Optimal RANSAC–Towards a Repeatable Algorithm for Finding the Optimal Set. *Journal of WSCG (Winter School of Computer Graphics)*, **21**(1), 21–30.

Jurgens, R. D. (1990). Realtime GPS Azimuth Determining System. *Proceedings of the National Technical Meeting of the Institute of Navigation*, San Diego, CA.

John, H. K. (2011). *Celestial Navigation in the GPS Age*. Arcata, Paradise Cay Publications, Inc.

Kaplan, G. H. (1999). New Technology for Celestial Navigation. *Proceedings: Nautical Almanac Office Sesquicentennial Symposium*, Washington D.C., CA.

Levine, S., Dennis, R., and Bachman, K. L. (1990). Strapdown Astro-Inertial Navigation Utilizing the Optical Wide-angle Lens Startracker. *Navigation*, **37**(4), 347–362.

Li, C., Zheng, Y., Yuan, Y., and Yang, Y. (2012a). Rapid Water-Sky-Line Detecting Algorithm in Marine Celestial Navigation. *The 3rd China Satellite Navigation Conference*, Guangzhou, CA.

Li, M., Jing X., and Huang X. (2012b). Autonomous Navigation for Lunar Satellite with Lunar Oblateness Correction. *Journal of Astronautics*, **33**(7), 896–902.

Li, C., Zheng, Y., Zhang, C., Yuan, Y., Lian, Y., and Zhou, P. (2014). Astronomical Vessel Position Determination Utilizing the Optical Super Wide Angle Lens Camera. *Journal of Navigation*, **67**(4), 633–649.

Li, C., Luo, Y., Zheng, Y., and Zhang, C. (2016). Research on Horizontal Line Fitting Algorithm Based on Robust Estimation. *The 7th China Satellite Navigation Conference*, Changsha, CA.

May, W. E. (1948). The Magnetic Compass: A Survey of Developments. *Journal of Navigation*, **1**(4), 342–353.

Ouyang, Z. (2005). *Introduction to Lunar Science*. Beijing, China Astronautic Publishing House.

Robbins, A. R. (2013). Geodetic Astronomy in the Next Decade. *Survey Review*, **24**(185), 99–108.

U.S. Naval Observatory. (2001). *Celestial Augmentation of Inertial Navigation Systems: A Robust Navigation Alternative*. San Diego, White Paper.

Wang, Y. (2006). *Fisheye Lens Optics*. Beijing, Science Press.
Yuan, Y. (2012). *Research on Fish-Eye Camera Stellar Calibration Technology*. Thesis (PhD), Zhengzhou Institute of Surveying and Mapping.
Zhan, Y., Zheng, Y., and Zhang, C. (2015). Astronomical Azimuth Determination by Lunar Observations. *Journal of Surveying Engineering*, **142**(2), 1–7.

APPENDIX

The components of Equation (26) are

$$\mathbf{V}=\begin{bmatrix} v_1 \\ v_2 \\ \cdots \\ v_j \\ \cdots \\ v_n \end{bmatrix} \quad \mathbf{A}=\begin{bmatrix} a_1 & b_1 \\ a_2 & b_2 \\ \cdots & \cdots \\ a_j & b_j \\ \cdots & \cdots \\ a_n & b_n \end{bmatrix} \quad \delta\hat{\mathbf{X}}=\begin{bmatrix} \delta\hat{\psi} \\ \delta\hat{\gamma} \end{bmatrix} \quad \mathbf{L}=\begin{bmatrix} L_1 \\ L_2 \\ \cdots \\ L_j \\ \cdots \\ L_n \end{bmatrix} \tag{A1}$$

where n denotes the number of points extracted from the horizon. The components of matrix **A** and vector **L** can be calculated as

$$a_j = \frac{2(z_{ch})_j \left(\frac{\partial z_{ch}}{\partial \hat{\psi}}\right)_0 ((x_{ch})_j^2+(y_{ch})_j^2) - 2(z_{ch})_j^2 \left((x_{ch})_j \left(\frac{\partial x_{ch}}{\partial \hat{\psi}}\right)_0 + (y_{ch})_j \left(\frac{\partial y_{ch}}{\partial \hat{\psi}}\right)_0\right)}{((x_{ch})_j^2+(y_{ch})_j^2)^2} \tag{A2}$$

$$b_j = \frac{2(z_{ch})_j \left(\frac{\partial z_{ch}}{\partial \hat{\gamma}}\right)_0 ((x_{ch})_j^2+(y_{ch})_j^2) - 2(z_{ch})_j^2 \left((x_{ch})_j \left(\frac{\partial x_{ch}}{\partial \hat{\gamma}}\right)_0 + (y_{ch})_j \left(\frac{\partial y_{ch}}{\partial \hat{\gamma}}\right)_0\right)}{((x_{ch})_j^2+(y_{ch})_j^2)^2} \tag{A3}$$

$$L_j = \frac{(z_{ch})_j^2}{(x_{ch})_j^2+(y_{ch})_j^2} - \frac{h^2+2Rh}{R^2} \tag{A4}$$

The components $\left(\frac{\partial x_{ch}}{\partial \hat{\psi}}\right)_0$, $\left(\frac{\partial y_{ch}}{\partial \hat{\psi}}\right)_0$, $\left(\frac{\partial z_{ch}}{\partial \hat{\psi}}\right)_0$, $\left(\frac{\partial x_{ch}}{\partial \hat{\gamma}}\right)_0$, $\left(\frac{\partial y_{ch}}{\partial \hat{\gamma}}\right)_0$ and $\left(\frac{\partial z_{ch}}{\partial \hat{\gamma}}\right)_0$ denote the initial values of $\frac{\partial x_{ch}}{\partial \hat{\psi}}$, $\frac{\partial y_{ch}}{\partial \hat{\psi}}$, $\frac{\partial z_{ch}}{\partial \hat{\psi}}$, $\frac{\partial x_{ch}}{\partial \hat{\gamma}}$, $\frac{\partial y_{ch}}{\partial \hat{\gamma}}$ and $\frac{\partial z_{ch}}{\partial \hat{\gamma}}$. They can be calculated as

$$\left(\frac{\partial x_{ch}}{\partial \hat{\psi}}\right)_0 = -(x_c)_j \sin\psi_0 + (y_c)_j \sin\gamma_0 \cos\psi_0 - (z_c)_j \cos\gamma_0 \cos\psi_0 \tag{A5}$$

$$\left(\frac{\partial y_{ch}}{\partial \hat{\psi}}\right)_0 = 0 \tag{A6}$$

https://doi.org/10.1017/S0373463318000073 Published online by Cambridge University Press

$$\left(\frac{\partial z_{ch}}{\partial \hat{\psi}}\right)_0 = (x_c)_j \cos\psi_0 + (y_c)_j \sin\gamma_0 \sin\psi_0 - (z_c)_j \cos\gamma_0 \sin\psi_0 \tag{A7}$$

$$\left(\frac{\partial x_{ch}}{\partial \hat{\gamma}}\right)_0 = (y_c)_j \sin\psi_0 \cos\gamma_0 + (z_c)_j \sin\psi_0 \sin\gamma_0 \tag{A8}$$

$$\left(\frac{\partial y_{ch}}{\partial \hat{\gamma}}\right)_0 = -(y_c)_j \sin\gamma_0 + (z_c)_j \cos\gamma_0 \tag{A9}$$

$$\left(\frac{\partial z_{ch}}{\partial \hat{\gamma}}\right)_0 = -(y_c)_j \cos\psi_0 \cos\gamma_0 - (z_c)_j \cos\psi_0 \sin\gamma_0 \tag{A10}$$

The components ψ_0 and γ_0 denote the initial values of the two attitude parameters.

https://doi.org/10.1017/S0373463318000073 Published online by Cambridge University Press